

## Review Article

## Open Access

B. Kuyken\*, F. Leo, S. Clemmen, U. Dave, R. Van Laer, T. Ideguchi, H. Zhao, X. Liu, J. Safioui, S. Coen, S.P. Gorza, S. K. Selvaraja, S. Massar, R. M. Osgood Jr., P. Verheyen, J. Van Campenhout, R. Baets, W.M. J. Green, and G. Roelkens

# Nonlinear optical interactions in silicon waveguides

DOI: 10.1515/nanoph-2016-0001

Received August 2, 2015; accepted November 5, 2015

**Abstract:** The strong nonlinear response of silicon photonic nanowire waveguides allows for the integration of nonlinear optical functions on a chip. However, the detrimental nonlinear optical absorption in silicon at telecom wavelengths limits the efficiency of many such experiments. In this review, several approaches are proposed

**\*Corresponding Author: B. Kuyken:** Photonics Research Group, Department of Information Technology, Ghent University–imec, Ghent, Belgium, E-mail: Bart.Kuyken@intec.ugent.be and Center for Nano- and Biophotonics (NB-Photonics), Ghent University, Ghent, Belgium

**S. Clemmen, U. Dave, R. Van Laer, H. Zhao, R. Baets, G. Roelkens:** Photonics Research Group, Department of Information Technology, Ghent University–imec, Ghent, Belgium and Center for Nano- and Biophotonics (NB-Photonics), Ghent University, Ghent, Belgium

**F. Leo:** Photonics Research Group, Department of Information Technology, Ghent University–imec, Ghent, Belgium and Center for Nano- and Biophotonics (NB-Photonics), Ghent University, Ghent, Belgium and Physics Department, The University of Auckland, Auckland, New Zealand

**S. Coen:** Physics Department, The University of Auckland, Auckland, New Zealand

**T. Ideguchi:** Research Centre for Spectrochemistry, University of Tokyo, Tokyo, Tokyo, Japan

**X. Liu:** Department of Optical Engineering and Quantum Electronics, College of Engineering and Applied Sciences, Nanjing Univ., Nanjing, 22 Hankou Rd Nanjing, Jiangsu PRC 210093, China

**J. Safioui:** Institut FEMTO-ST, Département d’Optique P. M. Duffieux, Université de Franche-Comté, Besançon, France

**S.P. Gorza:** OPERA-Photonique, Université Libre de Bruxelles (ULB), 50 Av. F. D. Roosevelt, CP 194/5, B-1050 Bruxelles, Belgium

**S. K. Selvaraja:** Centre for Nano Science and Engineering, Bengaluru, Indian Institute of Science, India

**S. Massar:** Laboratoire d’Information Quantique (LIQ) CP 224, Université libre de Bruxelles (U. L. B.), Bruxelles, Belgium

**R. M. Osgood Jr.:** Microelectronics Sciences Laboratories, Columbia University, New York, NY 10027, USA

**P. Verheyen, J. Van Campenhout:** imec, Kapeldreef 75, Leuven, Belgium

**W.M. J. Green:** IBM T. J. Watson Research Center, 1101 Kitchawan Road, Yorktown Heights, NY 10598, USA

and demonstrated to overcome this fundamental issue. By using the proposed methods, we demonstrate amongst others supercontinuum generation, frequency comb generation, a parametric optical amplifier, and a parametric optical oscillator.

## 1 Introduction

Silicon photonics is seen as a key enabling technology for the integration of highly complex optical circuits. The high index contrast allows for a high confinement and as such a small footprint for passive photonic circuits. The possibility of cointegrating fast, low-noise germanium photodetectors [1] and fast modulators [2], all with standard CMOS technology processes, make the platform highly attractive for the integration of active photonic networks. The silicon platform is now seen as the platform for optical interconnect applications in data centers [3].

Additionally, due to the high nonlinear response of the silicon nanophotonic waveguides, these structures attracted a significant interest from the nonlinear optics community. Indeed, in recent years, many research groups have demonstrated a large number of nonlinear optical functionalities such as supercontinuum generation [4], wavelength conversion [5] and all-optical signal processing [6] in silicon photonic wire waveguides. They were able to do this at very modest power levels because of the high nonlinear response of the silicon nanophotonic waveguides. Both silicon’s high linear and nonlinear refractive index contribute to the photonic wires’ strong nonlinear response. The most important reason being that silicon has a very high nonlinear refractive index, two orders of magnitude larger than that of silica [7]. Second, the tight confinement of silicon photonic wire waveguides (mode areas  $< 0.1 \mu\text{m}^2$ ) boosts the nonlinear response even further.

Despite the unrivaled nonlinear response of silicon photonic wire waveguides, silicon suffers from nonlinear absorption at telecom wavelengths [8]. The latter has lessened the initial enthusiasm for using this platform for non-



linear optics. However, there are a number of ways to reduce or get rid of the detrimental nonlinear absorption in the silicon waveguides. This article gives an overview of our recent work on the realization of nonlinear optical functions in silicon photonics with a focus on strategies that effectively avoid the detrimental nonlinear absorption.

The paper starts with a short introduction to nonlinear optics with an emphasis on the degenerate four wave mixing process, after which the most important results obtained in our group (through collaborative research) are discussed.

## 2 Nonlinear optics in silicon

In this article, we will focus mostly on the nonlinear response of materials caused by the nonlinear polarization of the electron cloud around the atoms. This function can be expanded in a Taylor series of the incident electric field:

$$P_{NL}(E) = \epsilon_0 \left( \chi^{(1)}E + \chi^{(2)}E^2 + \chi^{(3)}E^3 \dots \right). \quad (1)$$

It can be shown that in the bulk of a centrosymmetric material such as silicon the second order nonlinear response (the  $\chi^{(2)}$  term) is zero [9]. Despite the absence of the second order term, the third order term is very large in silicon. The strong third order term has several consequences, which will be used in this paper. The first is that the third order nonlinear response makes the refractive index intensity dependent. Second, the third order response allows for the so-called four-wave mixing process in which four optical waves interact.

The intensity dependence of the refractive index provides a straightforward parameter to quantify the nonlinearity of a material [10]:

$$n = n_0 + n_2 I. \quad (2)$$

However, the nonlinearity of a waveguide is even better quantified by its nonlinear parameter  $\gamma$ . Its real part is given by:

$$\gamma_{Re} = \frac{n_2 \omega}{A_{eff} c}. \quad (3)$$

The tighter the optical confinement in a waveguide, the stronger the electric field intensity in the waveguide is for given optical power. Therefore, this nonlinear parameter takes into account the effective mode area  $A_{eff}$  of the waveguide. The nonlinear parameter of silicon photonic wire waveguides and other Si-based waveguide platforms are shown in Table 1. It is clear that silicon waveguides have a very strong nonlinear response

compared to other Si-based waveguide materials systems. However, it needs to be emphasized that chalcogenide glass-based integrated platforms, albeit not CMOS compatible, show a very strong response: nonlinear parameters of up to  $136 \text{ W}^{-1} \text{ m}^{-1}$  have been measured at telecom wavelengths [11].

Nonetheless, silicon is prone to strong nonlinear absorption, i.e. two-photon absorption, at telecom wavelengths. In particular, although telecom photons ( $\sim 0.8 \text{ eV}$ ) cannot be absorbed under normal circumstances in silicon (silicon's bandgap is  $\sim 1.1 \text{ eV}$ ), nonlinear absorption can occur at high intensities. In this case the energy of two photons is used to bring an electron into the conduction band. The process is shown in Figure 1(a). This process also creates free carriers, which absorb light even more. The strong nonlinear absorption at telecom wavelengths, not present in materials with a larger bandgap, limits nonlinear interactions in crystalline silicon at these wavelengths. The nonlinear absorption is quantified by the imaginary part of the nonlinear parameter:

$$\gamma_{Im} = \frac{\alpha_2}{2A_{eff}}. \quad (4)$$

Here,  $\alpha_2$  is the two photon absorption coefficient ( $\alpha = \alpha_0 + \alpha_2 I$ , where  $\alpha$  is the total absorption coefficient,  $\alpha_0$  the linear absorption coefficient,  $I$  the intensity, and  $A_{eff}$  is the effective mode area).

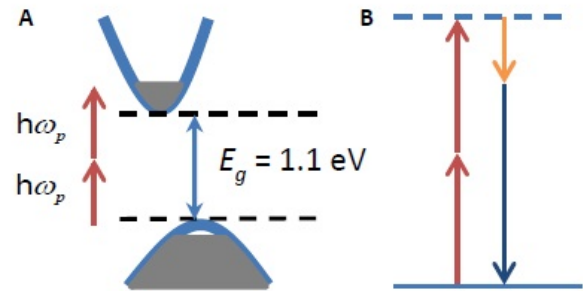


**Fig. 1.** (a) The two-photon absorption process: the combined energy of two photons generates a free carrier. (b) The degenerate four-wave mixing process in which a lower energy idler and high energy signal photon are created by the annihilation of two pump photons.

### 2.1 The degenerate four-wave mixing process

In the degenerate four wave-mixing process, two of the four interacting waves are degenerate. Hence, waves with only three distinct optical frequencies are involved in the

**Table 1.** The nonlinear refractive index and nonlinear parameter of some widely used Si-based materials and waveguide structures. Both the real and the imaginary part of the nonlinear parameter are given for a typical waveguide at 1.55  $\mu\text{m}$  wavelength.

	$n_2$ ( $10^{-20}$ m <sup>2</sup> /W)	$\gamma_{Re}$ ( $\text{W}^{-1}\text{m}^{-1}$ )	$\gamma_{Im}$ ( $\text{W}^{-1}\text{m}^{-1}$ )
Crystalline silicon waveguide [12]	650	450	150
Silicon nitride waveguide [13]	24	1.5	0
Hydex glass waveguide [14]	11.5	0.233	0
Silica fiber [10]	2.7	$10^{-3}$	0

process. In this process, energy is transferred from one wave to another. In this case, two pump photons are annihilated and a signal and idler photon are created as shown in Figure 1(b). As is clear from the figure, no energy is lost in the process. Energy conservation is not the only condition governing the process, the momentum also needs to be conserved. The latter condition is referred to as the phase-matching condition. These two conditions, stemming from the two conservation laws, are mathematically written as [10]:

$$\hbar\omega_p + \hbar\omega_p = \hbar\omega_i + \hbar\omega_s \Rightarrow \Delta\omega = \omega_s - \omega_p = \omega_p - \omega_i. \quad (5)$$

$$\beta_p + \beta_p = \beta_i + \beta_s + 2\gamma P \Rightarrow \beta_p = \frac{\beta_i + \beta_s}{2} + \gamma_{Re}P. \quad (6)$$

Here  $\hbar$  is Planck's constant,  $\omega_p$ ,  $\omega_i$ , and  $\omega_s$  are the pump, idler, and signal angular frequency respectively, and  $\beta_p$ ,  $\beta_i$  and  $\beta_s$  the pump, idler, and signal propagation constant respectively.  $\gamma$  is the nonlinear parameter of the waveguide and  $P$  the pump power. The term  $2\gamma P$  for phase matching (Eq. 6) takes into account the intensity dependent refractive index and the associated nonlinear phase shifts of the respective waves. The energy conservation condition shows that the detuning of the idler to the pump and the signal to the pump have to be equal. Additionally, the second condition shows that the propagation constant of the pump has to be close to the average of the propagation constant of the idler and signal. In fact, the propagation constant at the pump frequency needs to be slightly larger than the average of the signal and idler propagation constants to realize phase matching (assuming a positive  $n_2$ ). This condition can be satisfied in a waveguide. Indeed, in a waveguide, the dispersion—i.e., how the propagation constant  $\beta$  depends on the frequency  $\omega$  can be tailored.

## 2.2 Phase matching in silicon waveguides

As discussed above, phase matching is achieved by making sure that  $\beta_p = \frac{\beta_i + \beta_s}{2} + \gamma_{Re}P$ . To get some insight in how this can be achieved, it is instructive to expand the propagation constant as a function of the frequency in a Taylor

series in the vicinity of the pump:

$$\beta_i = \beta(\omega_i) = \beta_p - \Delta\omega\beta_{1p} + \frac{\Delta\omega^2}{2}\beta_{2p} - \frac{\Delta\omega^3}{6}\beta_{3p} + \frac{\Delta\omega^4}{24}\beta_{4p}. \quad (7)$$

$$\beta_s = \beta(\omega_s) = \beta_p + \Delta\omega\beta_{1p} + \frac{\Delta\omega^2}{2}\beta_{2p} + \frac{\Delta\omega^3}{6}\beta_{3p} + \frac{\Delta\omega^4}{24}\beta_{4p}. \quad (8)$$

Here  $\Delta\omega$  is the frequency detuning and  $\beta_{1p}$ ,  $\beta_{2p}$ ,  $\beta_{3p}$ , and  $\beta_{4p}$  are the first, second, third, and fourth order dispersion taken at the pump frequency. They are, respectively, the first, second, third, and fourth derivatives of the propagation constant with respect to the frequency at the pump wavelength. For small detuning, the terms in  $\beta_{3p}$  and  $\beta_{4p}$  can be neglected such that the phase matching condition becomes

$$\beta_{2p}\Delta\omega^2 + 2\gamma_{Re}P = 0. \quad (9)$$

The equation has a solution when  $\beta_{2p}$  is negative (for positive  $\gamma_{Re}$ ). This means that the group velocity dispersion has to be anomalous. Or, alternatively that the curvature of the function  $\beta(\omega)$  needs to be negative at the pump wavelength. Figure 2 shows a curve  $\beta(\omega)$  with a negative curvature at the pump wavelength such that  $\beta_p = \frac{\beta_i + \beta_s}{2} + \gamma_{Re}P$ .

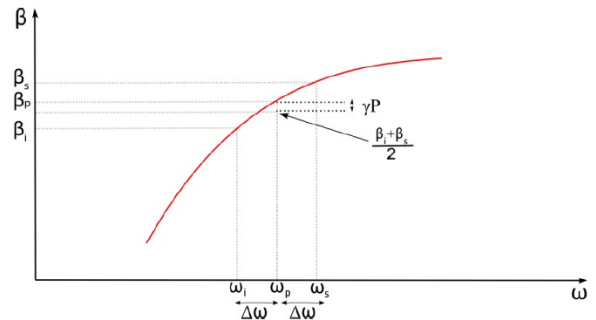


**Fig. 2.** Phase matching in the vicinity of the pump. The propagation constant as a function of the frequency has a negative curvature at the pump wavelength. Due to the negative curvature the phase matching condition can be satisfied.

The group velocity dispersion in silicon is strongly positive (normal) over a wide wavelength range (from 1.1  $\mu\text{m}$  up to  $\sim 5 \mu\text{m}$ ). However, the strong *waveguide* dispersion in highly confined silicon waveguides can offset the material dispersion. Hence, the total dispersion of a silicon waveguide can be engineered by tailoring the cross-section of the waveguide and phase matching can then be achieved [15–17].

The group velocity dispersion of a silicon waveguide as a function of wavelength can be verified using an interferometric setup [18]. As shown in Figure 3, a broadband source is sent to an interferometer and the fringes are recorded with an optical spectrum analyzer. The arms of the interferometer are balanced such that the group delay after passing through the chip and lensed fibers is equal to the group delay in the other (partly free space) arm. A 1550 nm fixed laser together with a photodiode and a PID controller are used to keep the arms balanced. It can be shown, when the arms are balanced for a specific wavelength, that the intensity of the fringes is given by [19]

$$I_{out}(\Delta\omega) = C_1 + C_2 \cos \left( C_3 - l_{wav} \left( \frac{1}{2} \beta_2 \Delta\omega^2 + \frac{1}{6} \beta_3 \Delta\omega^3 + \dots \right) \right). \quad (10)$$

Here,  $C_1$ ,  $C_2$ , and  $C_3$  are constants;  $l_{wav}$  is the waveguide length,  $\Delta\omega$  is the detuning parameter, and  $\beta_i$  are the waveguide dispersion terms. The fringe pattern is shown in Figure 4. From the fringe pattern, by balancing the interferometer at different wavelengths, the group velocity dispersion as well as the higher order dispersion terms can be measured. In this manner the dispersion of, for example, a partially underetched waveguide, with the cross-section shown in the inset of Figure 5 was measured. Partially etching the silicon oxide below the waveguide is done through a HF dip. The idea in this case is to finetune the dispersion of the waveguide by controlling the  $\text{SiO}_2$  etch. The group velocity dispersion of the fundamental TE mode for different etching times is also shown as a function of wavelength in Figure 5. The silicon waveguide itself is 860 nm wide and 217 nm thick.

### 2.3 Phase matching with the help of higher order dispersion terms

When higher order terms of the Taylor expansion (7, 8), i.e. up to the fourth order for simplicity, are taken into account equation (6) becomes:

$$\beta_{2p} \Delta\omega^2 + \beta_{4p} \frac{\Delta\omega^4}{12} + 2yP = 0. \quad (11)$$

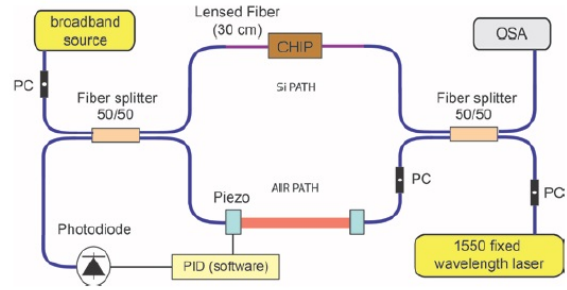


**Fig. 3.** A balanced interferometer to measure the group velocity dispersion of a waveguide. The interferometer is stabilized with the help of a 1550 nm laser. Adapted from reference [19].

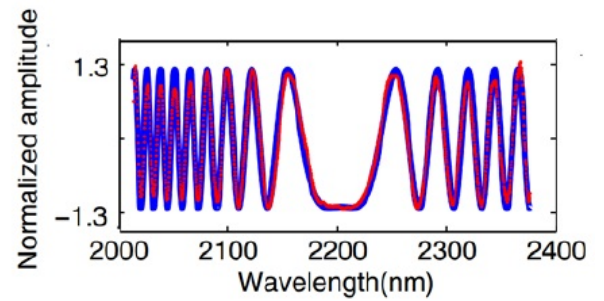


**Fig. 4.** The fringes recorded by the optical spectrum analyzer after the interferometer (red: recorded fringes; blue: fitted theoretical fringe pattern). The fringes allow to extract the dispersion profile of the waveguide. Adapted from reference [19].

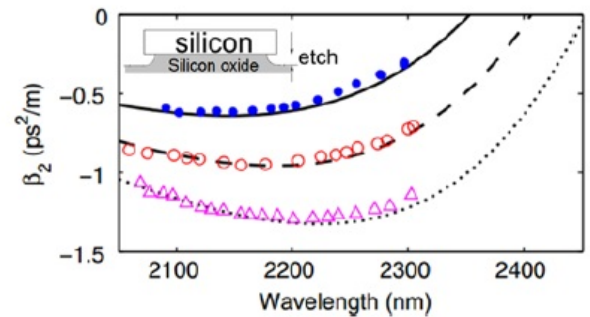


**Fig. 5.** The measured group velocity dispersion for waveguides, which are partially underetched by 0 nm (dots), 55 nm (circles) and 113 nm (triangles). Adapted from reference [19].

Assuming that the term  $2yP$  is small and positive, the equation can have two (degenerate) real solutions, one (degenerate) real solution or zero solutions depending on the signs of  $\beta_{2p}$  and  $\beta_{4p}$ . For a small detuning  $\Delta\omega$ , a solution can be found when  $\beta_{2p} < 0$ . This is the same solution as discussed above. When  $\beta_{4p} > 0$ , there is a second solution for larger detuning  $\Delta\omega$ . This situation is shown in Figure 6:



In our experiment, the silicon waveguide is pumped with short ( $\sim 150$  fs long, 30 nm wide FWHM) pulses centered at 1565 nm (TE polarization). Even in only a 7 mm long by 750 nm wide waveguide, the pulses (input peak power of 37 W) are broadened significantly as can be seen in Figure 9a. The spectrum of the output pulses spans (using the  $-30$  dB point) from 1160 nm up to 1700 nm. The peak around 1200 nm is believed to be the result of dispersive wave generation [20, 26].

Moreover, the wide spectrum, obtained by proper dispersion engineering, is found to be coherent. The pulse-to-pulse variations of the supercontinuum have been measured in an interferometric setup [27] shown in Figure 10. In the setup, a pulse is temporally overlapped with the next pulse and the optical spectrum is recorded. The deep fringes shown in Figure 9b demonstrate that the pulse-to-pulse variations are very limited, thus that the supercontinuum generation is highly coherent.

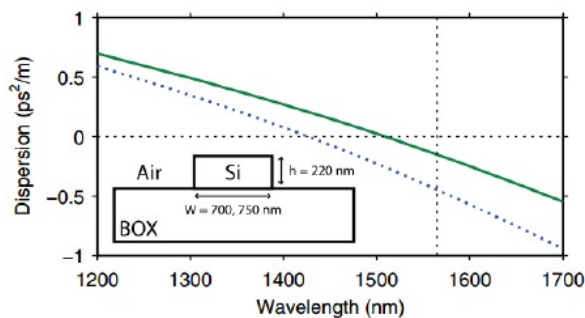


**Fig. 8.** The group velocity dispersion of the fundamental TE mode of a silicon waveguide as a function of wavelength for a 700 nm wide waveguide (dotted line) and a 750 nm wide waveguide (solid line). The inset shows the waveguide cross-section. Adapted from reference [26].

### 3.2 Noncrystalline silicon-based waveguide platforms

If one uses wider bandgap materials, two-photon absorption can be suppressed at short pump wavelengths. There have been several demonstrations of nonlinear experiments in silicon nitride integrated waveguides and hydrex waveguides [14]. Most notably, frequency comb generation [27–31]. However, the nonlinear parameter of such waveguides is relatively small. It is two orders of magnitude smaller than the value found in crystalline silicon (see Table 1).

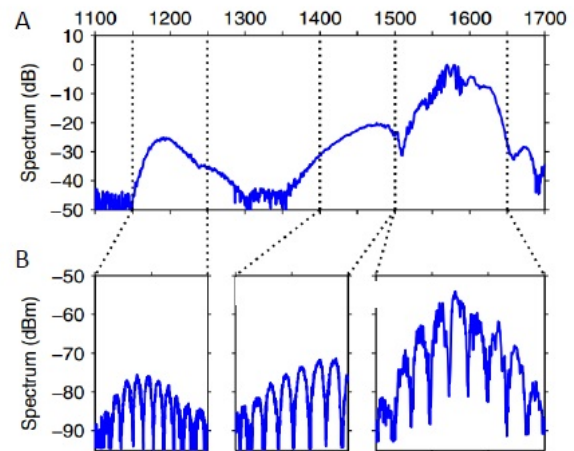


**Fig. 9.** Coherent supercontinuum generation in a silicon waveguide using fs pulses. a) The spectrum a) and b) the fringes obtained with the interferometric setup of Figure 10 show that the supercontinuum is coherent. Adapted from reference [26].

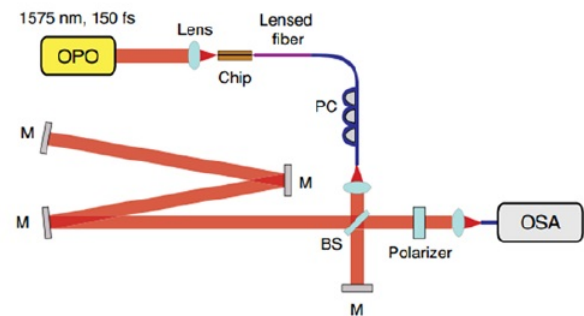


**Fig. 10.** Interferometric setup to measure the pulse to pulse coherence of the generated supercontinuum. Adapted from reference [26].

#### 3.2.1 Hydrogenated amorphous silicon

In several groups, including our own, hydrogenated amorphous silicon (a-Si:H) has been proposed as the material of choice for nonlinear interactions at telecom wavelengths. The material properties of a-Si:H strongly depend on the deposition process of the a-Si:H layers during fabrication [32]. Hence, different groups have reported different values for the nonlinear index and the two-photon absorption coefficient for the material at telecom wavelengths. However, as shown in Table 2, the real nonlinear response of a-Si:H waveguide structures can be very strong, with only limited two photon absorption at telecom wavelengths.

The first demonstration where the strong nonlinear response of a-Si:H has been exploited is a broadband optical parametric amplifier in the telecom wavelength band. The

amplifier consisted of a 500 nm wide air-clad waveguide fabricated in a 220 nm thick a-Si:H layer. The waveguide dispersion was measured to be anomalous ( $-2.6 \text{ ps}^2/\text{m}$ ) at the pump wavelength of 1535 nm [33]. The amplifier was able to amplify and convert ps signals pulses in a wavelength band ranging from  $\sim 1500 \text{ nm}$  to  $\sim 1590 \text{ nm}$ . The pulses were amplified by as much as 26.5 dB [38]. This is a more than 100-fold improvement over the best results in crystalline silicon [39] at this wavelength. In another experiment, the waveguides were also used in an all-optical signal processing experiment [33]. In this experiment, a 320 Gbit/s signal was sampled with an efficiency over 100 times stronger than could be achieved in crystalline silicon [40].

**Table 2.** The characteristics of several nonlinear a-Si:H waveguides reported in literature.

Reference	$n_2 (10^{-20} \text{ m}^2/\text{W})$	$\gamma_{Re} (\text{W}^{-1}\text{m}^{-1})$	$\gamma_{Im} (\text{W}^{-1}\text{m}^{-1})$
[33]	1300	770	28
[34]	4200	2000	482
[35]	50	35	14
[36]	7530	3000	434
[37]	2100	1200	70

In our group, we have observed that the a-Si:H layers are photo-sensitive when using telecom-band pump pulses. As a result, the nonlinear index reduces over time, while simultaneously increased linear losses are observed [33]. The material degradation of a-Si:H is a known phenomenon in the photovoltaic community and still not fully understood [41–43]. In another experiment, we have pumped the waveguides with photon energies well below the half-bandgap of our a-Si:H layers. In this experiment, a 1 cm long 800 nm wide waveguide with a thickness of 220 nm was pumped by a mode-locked thulium-doped fiber ps fiber laser operating at 1950 nm [44]. In those experiments, no degradation could be observed. Although more research is needed, these preliminary results indicate that two-photon absorption is likely related to the material degradation. Furthermore, it is interesting to note that in a set of experiments involving 150 fs pulses to generate a supercontinuum at telecom wavelengths [45], no degradation could be observed. However, it also needs to be emphasized that other groups have demonstrated a-Si:H waveguides, which are chemically stable at telecom wavelengths [36, 37]. These groups have shown a multitude of demonstrations of all-optical signal processing experiments in a-Si:H waveguides [36] and even as a source for photon pair generation [46, 47]. Lastly, by investigating the time-dependent response of hydrogenated amorphous

silicon waveguides, it has been observed that the Kerr-like response is far from instantaneous [48].

### 3.2.2 SiN waveguide structures for nonlinear optics in the visible/near-infrared

While SiN waveguide structures have a modest nonlinear parameter, they enable implementing nonlinear optical functions in the visible and near-infrared, where silicon is opaque. A multitude of linear and nonlinear functions in silicon nitride [14] have been demonstrated. However, most of these, such as supercontinuum generation [24] and comb generation [29, 31], have focused on the telecom wavelength band. In addition to this work, a broadband source covering red to near-infrared wavelengths is interesting for biophotonics applications. In this wavelength, band tissue and cells have a low absorption and the scattering loss is rather limited. Such a source could be useful for bio-imaging [49], optical coherence tomography [50] and Raman spectroscopy [51]. In fact, supercontinuum generation at these wavelengths in a silicon nitride waveguide was successfully demonstrated [52]. For this experiment, a partially underetched LPCVD  $\text{Si}_3\text{N}_4$  waveguide (similar as in the inset of Figure 5) was used. The waveguide was 500 nm wide and 300 nm high, the etch that removed the oxide below was 150 nm deep. By pumping such a 1 cm long waveguide with a Ti-Sapphire laser centered at 795 nm (FWHM 100 fs, 80 MHz repetition rate), an octave spanning supercontinuum from 488 to 978 nm (at  $-30 \text{ dB}$ ) was generated. Note that at this pump wavelength we do not expect any two-photon absorption in SiN.

## 3.3 Using pump photon energies smaller than or similar to the half bandgap energy in silicon

### 3.3.1 Introduction

Traditionally, the silicon photonics platform has been developed for the telecom wavelength window as applications were geared toward datacom and telecom [3, 53]. However, more recently researchers have explored other application directions for the platform. One of the most promising directions appears to be to use this technology for compact sensor chips. The availability of cheap, mass producible chips with a small form factor is attractive for many sensing applications. Several proof-of-principle sensing experiments [54, 55] have already been demonstrated using telecom wavelength light sources. However,

in a sensing context, it can be beneficial to shift the wavelength range of operation to the mid-infrared wavelength window (2–20  $\mu\text{m}$ ). In this wavelength window, many molecules have specific absorption spectra, which can be used as a fingerprint for the molecules. As a result the mid-infrared has been coined the molecular fingerprint region. The optical absorption of many molecules also tends to be much stronger in the mid-infrared as compared to that at telecom wavelengths. Hence, the development of integrated sources and detectors for the mid-infrared is currently an active field of research. Ideally, a mid-infrared sensing system should have a broadly tunable or broadband source and a low noise detector all operating at room temperature. These requirements are difficult to achieve, but can potentially be reached by using nonlinear optics as will be discussed below. Furthermore, by operating at lower optical frequencies with energies close to or below half the band gap of silicon two-photon absorption (and consequently free carrier absorption) is suppressed efficiently [8].

### 3.3.2 Linear properties of silicon waveguides in the mid-infrared

The standard silicon waveguides offered by multiproject wafer services have a fixed height of 220 nm on a buried oxide layer of 2  $\mu\text{m}$ . Such waveguides fail to possess good confinement when operated at long wavelengths and as a consequence the guided mode leaks into the substrate. For example, Figure 11(a) shows the simulated substrate loss as a function of wavelength for the fundamental TE mode of a 900 nm wide waveguide. Although such a waveguide structure can be used for wavelengths up to  $\sim 3000$  nm, the losses become too high at longer wavelengths. Hence, a thicker waveguide layer is needed to guide longer wavelengths. The simulated substrate loss for the fundamental TE mode of a 1300 and 1500 nm wide strip waveguide etched in a 400 nm thick silicon layer is shown in Figure 11(b). As shown in the figure, the losses remain low up to  $\sim 4000$  nm. Therefore, such waveguides allow for using the whole transparency region of the SOI platform. At short wavelengths the transparency is limited by the absorption in silicon at 1100 nm and at long wavelengths by the absorption of the buried oxide at  $\sim 4000$  nm. Furthermore, the thick waveguides allow for more flexibility in dispersion engineering. In short, for wavelengths up to 3000 nm standard 220 nm thick device layer SOI wafers can be used, however when working at longer wavelengths thicker device layer wafers are required.

### 3.3.3 A mid-infrared optical parametric amplifier

A first and clear demonstration of the strong nonlinear response of silicon waveguides in the mid-infrared is provided by the realization of a silicon mid-infrared optical parametric amplifier. At the core of the amplifier is a 900 nm wide crystalline silicon waveguide with a height of 220 nm and 2 cm length. The dispersion of the silicon nanowire waveguide is shown in Figure 12. As shown in the figure, the group velocity dispersion is anomalous from 1810 to 2410 nm (TE polarization). We chose 2120 nm, in the middle of the anomalous region, as the pump wavelength. The pump generates a pulse train with pulses estimated to be 2 ps long. These are generated by an optical parametric oscillator (Coherent Mira-OPO, repetition rate = 76 MHz) in the experiment. The output spectrum, after passing through 2 cm waveguide, is shown in Figure 13(a). As can be seen in the figure, a broad spectrum is generated from  $\sim 1920$  nm to 2450 nm. The broad spectrum is the result of spontaneous four-wave mixing in which pairs of idler and signal photons are generated, a phenomenon sometimes referred to as modulation instability. The two peaks, one at 2411 nm and one at 1950 nm are the result of Raman gain in silicon [56]. In a following experiment, the amplifier is seeded with a CW laser. In the four-wave mixing process, the CW laser is amplified, but also converted to another wavelength. The measured amplification, taking in account the duty cycle of the pulsed source in the band 2200 nm to 2500 nm, is shown in Figure 13(b). The amplification, when the region of the Raman Stokes frequency is probed, can reach 50 dB. Overall the amplifier showed net-gain including the insertion loss of the chip over a 550 nm band.

### 3.3.4 A mid-infrared wavelength translator

A wavelength translator allows for bridging gaps between different wavelength bands [59–62]. This can be beneficial in situations where sources and detectors are more developed in one band compared to the other. Here, we show how we can translate telecom signals (generated by high-performance sources) to the mid-infrared and back. Translating mid-infrared signals to the telecom wavelength range makes it possible to detect the signals with room temperature-sensitive, low-noise, and high-speed telecom detectors, devices that are not readily available in the mid-infrared [63].

It is possible (see Section 2.4) to achieve phase matching in the degenerate four-wave mixing process in a discrete band for large signal an idler detuning. However,

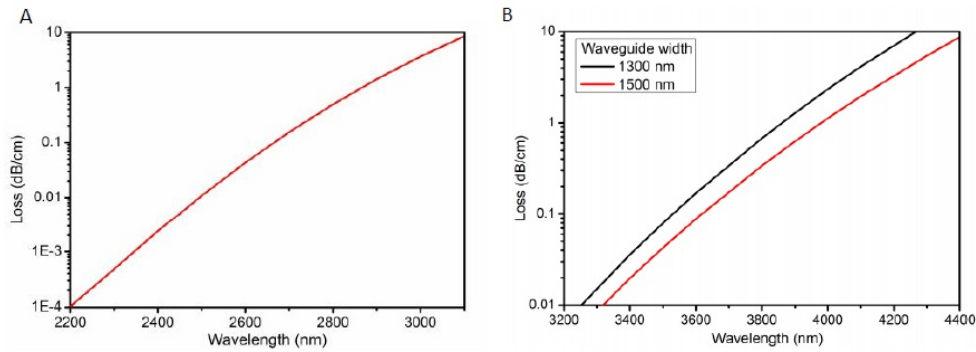


**Fig. 11.** (a) Substrate leakage of a 900 nm wide air-clad strip waveguide with a height of 220 nm (fundamental TE mode) as a function of wavelength; (b) substrate leakage loss of a 1300 and 1500 nm wide strip waveguide, etched in a 400 nm thick silicon waveguide layer as a function of wavelength (fundamental TE mode).

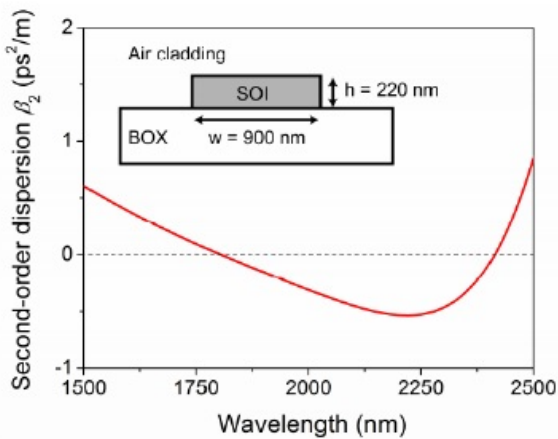


**Fig. 12.** The group velocity dispersion of the waveguide used for the mid-infrared parametric amplifier experiment as well as for the OPO experiment discussed in Section 3.3. The inset shows a cross-section of the waveguide. Adapted from reference [57].

the sign of the second and fourth order dispersion coefficients have to be opposite for this to happen. Figure 14 shows these dispersion parameters for a 900 nm wide silicon waveguide with an air cladding fabricated in a 220 nm thick silicon layer. The second order dispersion is negative in a range from 1810 to 2410 nm while the fourth order coefficient dispersion is positive. Moreover, because the second order dispersion is negative phase-matching is also obtained in the vicinity of the pump wavelength. Since the second order and fourth order dispersion coefficients are wavelength dependent, the discrete phase-matching bands are also dependent on the pump wavelength. The experimentally obtained location of the discrete bands is shown as a function of the pump wavelength in Figure 15. In the experiments the pump (2 ps FWHM, 82 MHz) is centered at 1946 nm. The chosen pump wave-

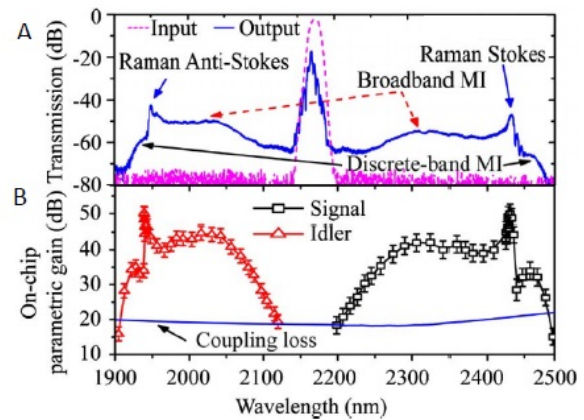


**Fig. 13.** Parametric amplification in the mid-infrared using the waveguide described in Fig. 12, pumped using ps pulses centered around 2120 nm. (a) The spectrum of the pump pulses before and after passing through a 2 cm long waveguide; (b) amplification and conversion efficiency as a function of seed wavelength. The total insertion loss of the chip is shown in blue. Adapted from reference [58].

length allowed for phase matching between the pump and a signal and idler in a band around 1620 and 2440 nm. By converting a CW laser at 2440 nm to the telecom wavelength band, the functionality of the wavelength translator is shown in Figure 16. When the pump power was 37 W conversion efficiencies of  $\sim 20$  dB were obtained. The conversion efficiency as a function of wavelength is shown in Figure 17. Furthermore, it is also shown that telecom signals in a band around 1620 nm can be converted to the mid-IR band albeit with a lower efficiency. The latter is attributed to the higher cross-TPA between the pump and the telecom probe.

Following up on these experiments, the span over which the translator works was increased by proper op-

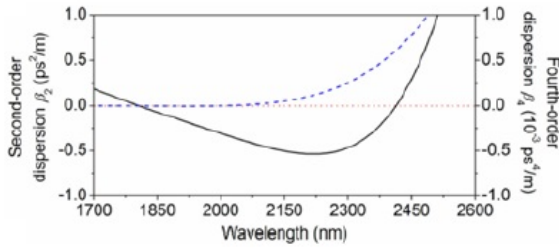


**Fig. 14.** The simulated second (black line) and fourth order (blue dashed line) dispersion of the 900 nm wide silicon waveguide. The sign of the second and fourth order dispersion are opposite in a band between 1810 and 2410 nm. Adapted from reference [63].

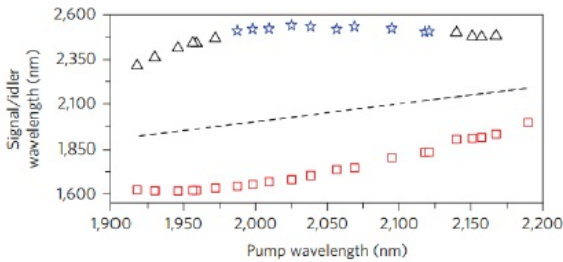


**Fig. 15.** The phase-matched signal (squares) and idler (stars and triangles) wavelengths as a function of the pump wavelength in the four wave mixing process in the silicon waveguide. The stars represent the calculated idler location (from the measured signal wavelength) as they are outside the bandwidth of the OSA. Adapted from reference [63].

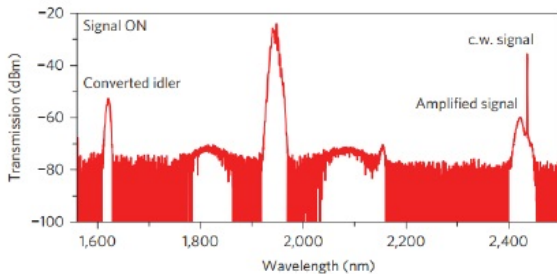


**Fig. 16.** The output spectrum after the signals (1946 nm pump pulses and a 2440 nm CW signal) have propagated through the silicon waveguide. In this case, the mid-infrared CW signal is converted to the telecom wavelength band. Adapted from reference [63].

timization of the dispersion of the waveguide. Moreover, by using a waveguide with a positive second order dispersion and a negative fourth order dispersion phase matching in the vicinity of the pump is suppressed. As a consequence, the spontaneous four wave mixing (modulation instability) is suppressed. This reduces the noise of the translator significantly [64]. In the experiment presented here, a waveguide is etched in a 390 nm thick silicon de-

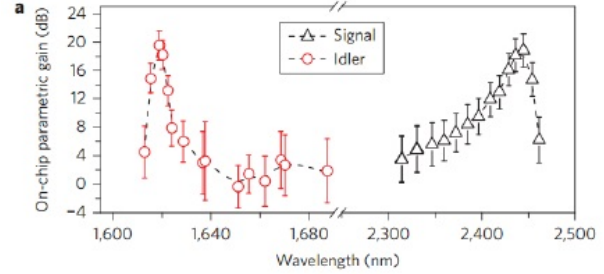


**Fig. 17.** Amplification and conversion efficiency of the silicon wavelength translator (see Figs. 15 and 16) as a function of the mid-infrared signal wavelength. Adapted from reference [63].

vice layer. The cross-section of the waveguide is shown in the inset of Figure 18(a). As can be seen in the figure, the waveguide is slightly over etched such that also 10 nm of silica is also removed. The dispersion of the fundamental TE mode of the waveguide is shown in Figure 18(a). As can be seen in the figure the second order dispersion of the waveguide is positive for wavelengths shorter than 2275 nm, while at the same time the fourth-order dispersion of the waveguide is negative. As such the waveguide allows for phase-matching signal and idler frequencies with the pump wavelength in discrete bands. In the experiment, a 1 cm long waveguide is used, and the pump wavelength is swept over a narrow wavelength range. The subsequent spectral peaks of spontaneous light generation resulting from the process of modulation instability reveal the location of the phase-matched bands. The peak wavelength of these bands is shown in Figure 18(b) as a function of pump wavelength. The experimental points agree well with the simulated curve that links the phase-matched signal and idler waves with the pump wavelength. Next, the wavelength translator is used to translate a signal from the telecom band into the mid-IR. The pump pulses are centered at 2190 nm (2 ps 76 MHz) such that a telecom signal at 1565 nm is converted to an idler wavelength at 3635 nm. For the experiment the ps pulse train is combined with a telecom CW laser in a 90/10 splitter and coupled into the fundamental TE mode of the silicon waveguide with the help of a lensed fiber. The light is coupled out of the waveguide with a chalcogenide lens. The spectrum at the output of the waveguide is characterized with an FTIR. However, due to the limited dynamic range of the FTIR, the light is first sent through a long pass filter to suppress the pump. The converted idler at 3635 nm can be seen in the output spectrum shown in Figure 19. The translator is not only able to translate the light over more than an octave, it also allows amplification of the telecom signal. Indeed, when the output from the wavelength translator is sent to a fast telecom

photodetector the telecom CW light is amplified when it is temporally overlapping with the ps pump pulses. Figure 20 shows a time trace of the telecom signal. The amplification is calculated to be 12 dB.

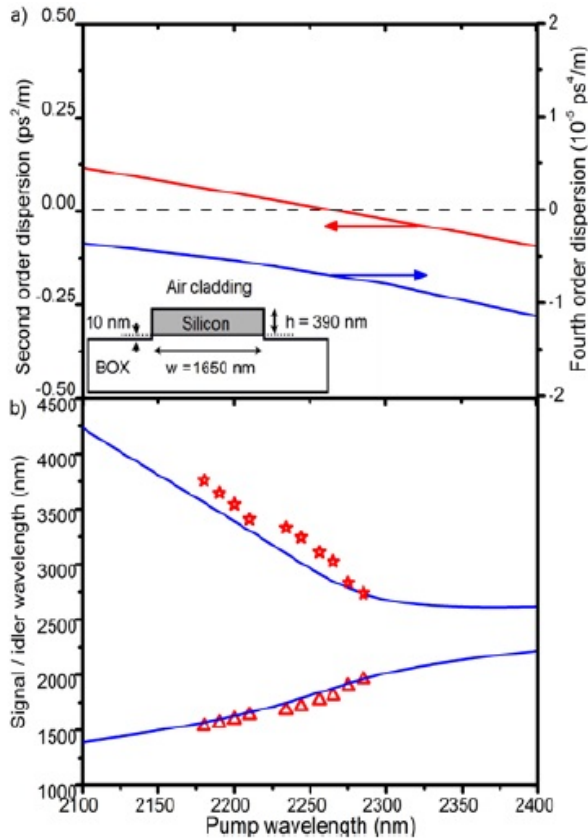


**Fig. 18.** (a) The simulated second and fourth order dispersion of the silicon waveguide shown in the inset. (b) The phase-matched signal (triangles) and idler (stars) wavelengths as a function of the pump wavelength for this waveguide. The blue line is the theoretical prediction of phase-matched idler and signal pairs as a function of pump wavelength. Adapted from reference [65].

### 3.3.5 Broadband light generation in a silicon chip

The process of supercontinuum generation allows one to generate a broadband signal from a narrowband source as shown above. Here, we show the generation of a supercontinuum in a silicon waveguide with a very high nonlinear parameter in the mid-infrared. The waveguide that was used is 900 nm wide and fabricated in a 220 nm thick layer of silicon. Its dispersion is shown in Figure 12. It is anomalous at the pump wavelength of 2120 nm. Again 2 ps pulses generated by the external OPO are used as a

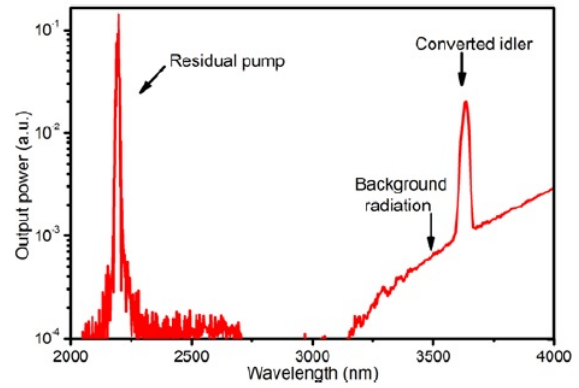


**Fig. 19.** The output spectrum of the wavelength translator when it is seeded with a CW probe at 1565 nm. A strong signal at 3635 nm can be seen above the thermal background of the detector. Adapted from reference [65].

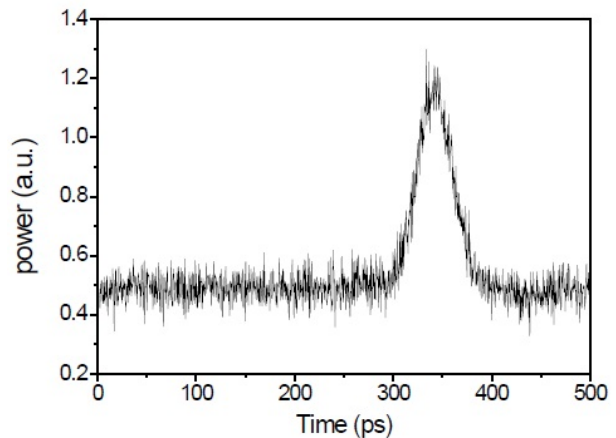


**Fig. 20.** Amplification of a telecom probe. A temporal trace recorded by a fast photo-detector in the telecom band. The instantaneous amplification after propagating through the silicon waveguide visible (shown in the inset of Figure 18) of the telecom probe signal is clearly visible.

pump. Coupling in and out of the waveguide is done with lensed fibers. The output spectrum when the waveguides are pumped with 13.7 W peak power pulses is shown in Figure 21. The spectrum (at  $-30$  dB) spans from 1530 nm to beyond 2500 nm.

While such a supercontinuum source is spatially coherent (all light is coupled to a single electromagnetic mode), it is not temporally coherent. A supercontinuum source, which is generated by pumping the waveguide with ps long pulses, relies primarily on the amplification of background noise through the process of modulation instability. The process is well known to destroy the coherence of the supercontinuum [10]. The pulse to pulse

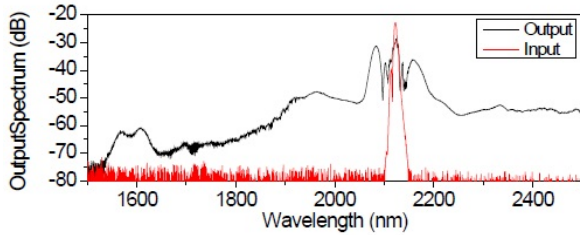


**Fig. 21.** Supercontinuum generation in a 900 nm wide and 220 nm thick silicon waveguide. The input and output spectrum of the pulse train shows the dramatic spectral broadening of the pulses after propagating through a 2 cm long nanowire waveguide. Adapted from reference [57].

variations are significant because the process is seeded by noise.

### 3.3.6 Coherent mid-infrared supercontinuum generation: Frequency combs

The temporal coherence of a supercontinuum can be maintained by pumping nonlinear waveguides with ultrashort pulses. The process of spectral broadening of ultrashort pulses favors the so-called soliton fission, which preserves the coherence [20]. The pulse to pulse variation is very limited. Therefore a temporally coherent supercontinuum is created. Such a coherent supercontinuum has a comb-like spectrum. Such sources are of importance for the field of dual comb spectroscopy. They allow for measuring absorption spectra at very high acquisition rates and therefore allow doing real-time spectroscopy over a broad wavelength range. Expanding the available (commercial) frequency combs into the mid-infrared would be of interest for spectroscopic applications in the mid-infrared.

For our experiments, a silicon waveguide with a cross-section similar to that shown in Figure 18, but having a width of 1600 nm, is used. The waveguide is pumped with a 100 MHz ~60 fs pulse train coming from an OPO and coupled to the chip with the help of chalcogenide lenses. The output of the waveguide is coupled to a FTIR. When the waveguide is pumped with a 225 W peak power pulse train the spectrum spans from 1540 nm up to 3200 nm see Fig. 22 (at the -30 dB level) [66]. Next, the comb structure and as such the coherence of the supercontinuum is verified. For this purpose, the spectrum of the supercontinuum is combined with a narrow linewidth CW laser. The beat note of the supercontinuum and a 1586 nm laser is shown in Figure 23. A narrow line width beat note revealed the comb structure of the spectrum. The experiment is repeated at

2418 nm and 2580 nm. Again narrow line width beat notes are obtained.

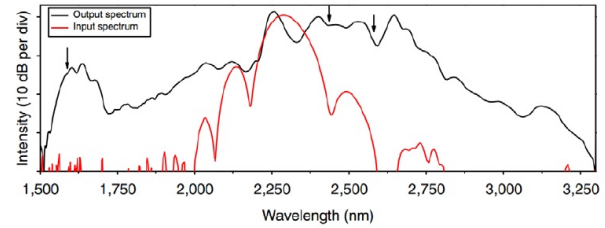


**Fig. 22.** An octave spanning coherent supercontinuum. The spectrum of the 60 fs long, 225 W peak power pump pulses is spectrally broadened over more than an octave in a 1 cm long, 1600 nm wide and 390 nm high, slightly overetched waveguide. Adapted from reference [66].

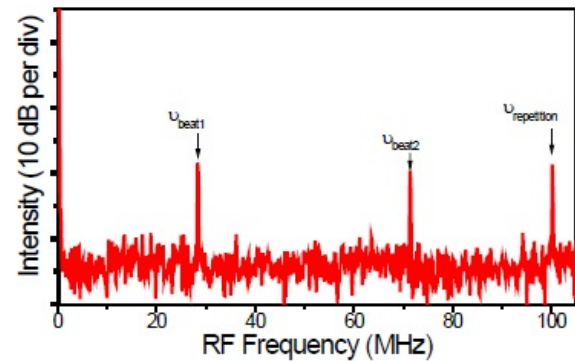


**Fig. 23.** Narrow linewidth beat notes illustrating the temporal coherence of the supercontinuum shown in Fig. 22 notes illustrating the temporal coherence of the supercontinuum. Adapted from reference [66].

### 3.3.7 Synchronously pumped optical parametric oscillator

The broadband gain of the silicon waveguides can be exploited to make a tunable short pulse source. Here we show how a silicon-based optical parametric oscillator (OPO) can be constructed. Unlike a more traditional OPO, where a second order nonlinear crystal is used, the nonlinear element here is a  $\chi^{(3)}$  silicon waveguide. The high gain that can be obtained in such a silicon waveguide is sufficient to overcome the round-trip losses when it is placed in a cavity. Here, a 2 cm long 900 nm waveguide is used as the nonlinear gain element. The cross-section of the waveguide and the dispersion is shown in Figure 12. In a first experiment, the single pass amplification of the waveguides

is measured, using the method and pump as in the previous section. The single pass gain is shown in Figure 24. Next, the silicon chip is placed in a cavity built with single-mode fiber. A schematic of the fiber loop around the silicon gain element is shown in the inset of Figure 24. The round-trip loss of the loop is shown in Figure 24 in blue. The round-trip loss is relatively high, primarily because of the high in and out-coupling losses of the chip, but also as a result of the substantial loss of the delay line. Despite the high losses, there are broad regions where the single pass gain overcomes the linear round trip losses. In these regions oscillation is possible. Experimentally, this is verified and the output pulses of the silicon based OPO are shown in the inset of Figure 25. Broadband tuning is obtained by exploiting the high dispersion of the single-mode fiber in the mid-infrared. The delay-line is changed such that the round-trip time of the cavity is matched with the pulse repetition rate for a particular idler wavelength. The output power as a function of the wavelength is shown in Figure 25. Interestingly, due to the favorable nonlinear properties of hydrogenated amorphous silicon also widely tunable OPOs have been demonstrated using a-Si:H [67].

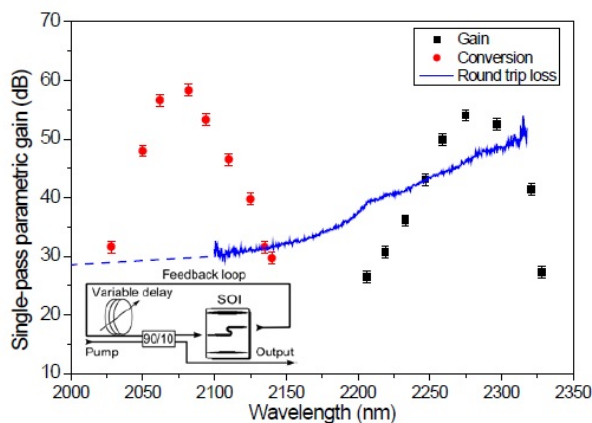


**Fig. 24.** The parametric gain of the photonic wire waveguide and the round trip-losses of the cavity. The gain can overcome the losses over a broad wavelength band. The inset shows a schematic of the experimental setup. The cross-section of the waveguide is the same as shown in the inset of Figure 12. Adapted from reference [68].

### 3.4 Non-Kerr nonlinearities in silicon

Several researchers have tried to incorporate second order nonlinearities in silicon waveguides. To achieve this goal, the inversion symmetry in the silicon crystal has to be broken. The most efficient approach involves the straining of

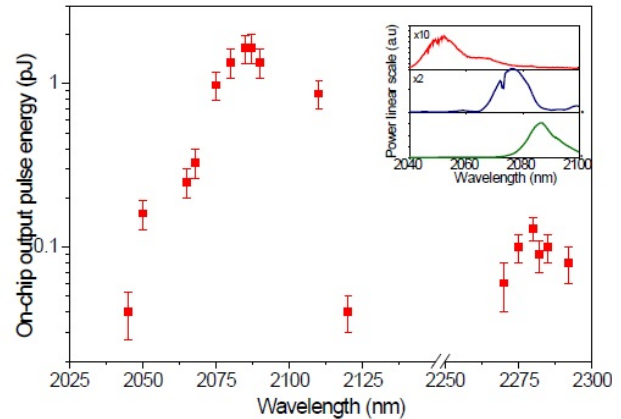


**Fig. 25.** The output power of our OPO, as shown in the inset of Fig. 24 at different idler wavelengths. Adapted from reference [68].

the silicon waveguides, e.g. with a strained silicon nitride overlay. As such a silicon pockets effect modulator [69] and second harmonic generation [70] has been demonstrated in a silicon waveguide. Another approach for enhancing the nonlinear response of silicon waveguides is by making use of the strong photon–phonon coupling that can be achieved in these waveguides using stimulated Brillouin scattering. Recently, the strong coupling of the photons in a silicon waveguide with the phonons in a silicon–nitride membrane has been observed [71]. In our group, we have expanded this concept and demonstrated ultra-strong coupling of photons and phonons in the same silicon nanophotonic waveguide [72]. Although these nonlinear interactions are narrow band (several tens of MHz), they can be relatively strong. As such net-optical CW gain can be achieved in silicon waveguides [73]. Furthermore, the narrow bandwidth can be interesting for microwave photonics applications [74].

## 4 Conclusions

The silicon-on-insulator platform is a very promising platform for integrating nonlinear optical functions. The high refractive index of silicon combined with the high confinement of silicon waveguides allows for a large nonlinear parameter. Furthermore, the strong confinement enables broadband dispersion engineering. As such, a number of devices, for which efficient nonlinear four-wave mixing was enabled by phase matching, have been demonstrated. In this paper, we have shown parametric amplification, parametric oscillation, and supercontinuum generation in silicon waveguides. Despite the strong nonlinear absorption at telecom wavelengths, efficient nonlinear functions

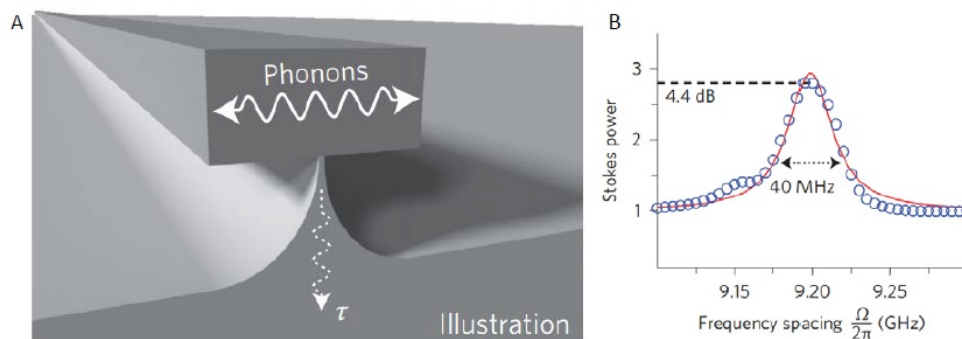


**Fig. 26.** Phonon-photon coupling in a silicon photonic waveguide. (a) Illustration of the partially underdetuned waveguide. (b) The on/off gain of a detuned signal by a 35 mW pump.

in the telecom window can be achieved by moving towards silicon-like platforms such as hydrogenated amorphous silicon and silicon nitride, which have a wider bandgap or by using ultrashort pulses. In crystalline silicon, the best results are achieved when one uses pump photons with an energy close or smaller than the half bandgap of silicon. The results obtained by using long wavelength pumps are useful in a sensing context, where one prefers to work at longer wavelengths as the absorption of many molecules is much stronger there as compared to the telecom wavelength window. The nonlinear interactions in silicon allow meeting the demand of delivering widely tunable or broadband sources in this wavelength window.

## References

- [1] Chen L, Lipson M Ultra-low capacitance and high speed germanium photodetectors on silicon. *Optics Express* 2009, 17, 7901-7906.
- [2] Reed G, Mashanovich G, Gardes FY, Thomson DJ Silicon optical modulators *Nature photonics* 2010, 4, 518-526.
- [3] Gunn C, CMOS photonics for high-speed interconnects *IEEE Proc Comput Sci* 2006, 26, 58-66
- [4] Hsieh I-W, Xiaogang C, Xiaoping L, Dadap, Panoiu N, Chou C, Xia F, Green WM, Vlasov YA, Osgood RM, Supercontinuum generation in silicon photonic wires *Optics express* 2007, 15, 15242-15249.
- [5] Foster MA, Turner AC, Salem R, Lipson M, Gaeta AL Broad-band continuous-wave parametric wavelength conversion in silicon nanowaveguides *Optics Express* 2007, 15, 12949-12958.
- [6] Li F, Pelusi M, Xu DX, Densmore A, Ma R, Janz S, Moss DJ Error-free all-optical demultiplexing at 160Gb/s via FWM in a silicon nanowire *Optics Express* 2010, 18, 3905-3910.
- [7] Dinu M, Quochi F, Garcia H Third-order nonlinearities in silicon at telecom wavelengths *Applied Physics Letters* 2003, 82, 2954-2956.
- [8] Bristow AD, Rotenberg N, Van Driel HM Two-photon absorption and Kerr coefficients of silicon for 850-2200 nm *Appl. phys. Lett* 2007, 90, 191104.
- [9] Boyd RW *Nonlinear optics*, Academic press, 2003.
- [10] Agrawal GP *Nonlinear Fiber Optics*, Academic press, 1995.
- [11] Gai X, Madden S, Choi DY, Bulla D, Luther-Davies B Dispersion engineered Ge<sub>11.5</sub>As<sub>24</sub>Se<sub>64.5</sub> nanowires with a nonlinear parameter of 136 W<sup>-1</sup> m<sup>-1</sup> at 1550 nm *Optics express* 2010, 18, 18866-18874.
- [12] Osgood RM Jr., Panoiu NC, Dadap J, Liu X, Chen X, Hsieh IW, Dulkeith E, Green WM, Vlasov YA Engineering nonlinearities in nanoscale optical systems: physics and applications in dispersion engineered silicon nanophotonic wires *Adv. Opt. Photon.* 2009, 1, 162-235.
- [13] Tan DTH, Ikeda K, Sun PC, Fainman Y Group velocity dispersion and self phase modulation in silicon nitride waveguides *Appl. Phys. Lett.* 2010, 96, 061101-061103.
- [14] Moss DJ, Morandotti R, Gaeta AL, Lipson M New CMOS-compatible platforms based on silicon nitride and Hydex for nonlinear optics *Nat. Photonics* 2013, 7, 597-607.
- [15] Liu X, Green WMJ, Chen X, Hsieh IW, Dadap JI, Vlasov YA, Osgood RM Jr. Conformal dielectric overlayers for engineering dispersion and effective nonlinearity of silicon nanophotonic wires *Optics letters* 2008, 33, 2889-2891.
- [16] Foster MA, Salem R, Geraghty DF, Turner-Foster AC, Lipson M, Gaeta AL Silicon-chip-based ultrafast optical oscilloscope *Nature* 2008, 456, 81-84.
- [17] Lau RKW, Ménard M, Okawachi Y, Foster MA, Turner-Foster AC, Salem R, Lipson M, Gaeta AL Continuous-wave mid-infrared frequency conversion in silicon nanowaveguides *Optics letters* 2011, 36, 1263-1265.
- [18] Peterka P, Kaňka J, Honzátko P, Káčik D Measurement of chromatic dispersion of microstructure optical fibers using interferometric method *Opt. Appl* 2008, 38, 295-303.
- [19] Leo F, Dave U, Keyvaninia S, Kuyken B, Roelkens G Measurement and tuning of the chromatic dispersion of a silicon photonic wire around the half band gap spectral region *Optics Letters* 2014, 39, 711-714.
- [20] Dudley JM, Genty G, Coen S Supercontinuum generation in photonic crystal fiber *Reviews of Modern Physics* 2006, 78, 1135.

- [21] Husakou, A. V., and J. Herrmann. "Supercontinuum generation of higher-order solitons by fission in photonic crystal fibers." *Physical Review Letters* 87, no. 20 (2001): 203901.
- [22] Kano H, Hamaguchi H Dispersion-compensated supercontinuum generation for ultrabroadband multiplex coherent anti-Stokes Raman scattering spectroscopy *Journal of Raman Spectroscopy* 2006, 37, 411-415.
- [23] Humbert G, Wadsworth W., Leon-Saval S, Knight J, BirkT, Russell P, Lederer L, Supercontinuum generation system for optical coherence tomography based on tapered photonic crystal fibre *Optics Express* 2006, 14, 1596-1603.
- [24] Halir R, Okawachi Y, Levy JS, Foster MA, Lipson M, Gaeta AL Ultrabroadband supercontinuum generation in a CMOS-compatible platform *Optics Letters* 2012, 37, 1685-1687.
- [25] Yu Y, Gai X, Wang T, Ma P, Wang R, Yang Z, Choi DY, Madden S, Luther-Davies B Mid-infrared supercontinuum generation in chalcogenides *Optical Materials Express* 2013, 3, 1075-1086.
- [26] Leo F, Gorza SP, Coen S, Kuyken B, Roelkens G Coherent supercontinuum generation in a silicon photonic wire in the telecommunication wavelength range *Optics Letters* 2015, 40, 123-126.
- [27] Gu X, Kimmel M, Shreenath A, Trebino R, Dudley J, Coen S, Windeler R Experimental studies of the coherence of microstructure-fiber supercontinuum *Optics Express* 2003, 11, 2697-2703.
- [28] Levy J, Gondarenko A, Foster MA, Turner-Foster AC, Gaeta AL, Lipson M CMOS-compatible multiple-wavelength oscillator for on-chip optical interconnects *Nature Photonics* 2010, 4, 37-40.
- [29] Okawachi Y, Saha K, Levy JS, Wen H, Lipson M, Gaeta AL Octave-spanning frequency comb generation in a silicon nitride chip *Optics Letters* 2011, 36, 3398-3400.
- [30] Razzari L, Duchesne D, Ferrera M, Morandotti R, Chu S, Little BE, Moss DJ CMOS-compatible integrated optical hyperparametric oscillator *Nature Photonics* 2010, 4, 41-45.
- [31] Herr T, Hartinger K, Riemensberger J, Wang CY, Gavartin E, Holzwarth R, Gorodetsky ML, Kippenberg TJ Universal formation dynamics and noise of Kerr-frequency combs in microresonators *Nature Photonics* 2012, 6, 480-487.
- [32] Street R, *Hydrogenated amorphous silicon*, Cambridge University Press, 2005.
- [33] Kuyken B, Ji H, Clemmen S, Selvaraja SK, Hu H, Pu M, Galili M Nonlinear properties of and nonlinear processing in hydrogenated amorphous silicon waveguides *Optics Express* 2011, 19, B146-B153.
- [34] Narayanan K, Preble SF Optical nonlinearities in hydrogenated-amorphous silicon waveguides *Optics Express* 2010, 18, 8998-9005.
- [35] Shoji Y, Ogasawara T, Kamei T, Sakakibara Y, Suda S, Kintaka K, Kawashima K, Okano, Hasama T,
- [36] Wang KY, Foster AC Ultralow power continuous-wave frequency conversion in hydrogenated amorphous silicon waveguides *Optics Letters* 2012, 37, 1331-1333.
- [37] Grillet C, Carletti L, Monat C, Grosse P, Bakir B, Menezo S, Fedeli JM, Moss DJ Amorphous silicon nanowires combining high nonlinearity, FOM and optical stability *Optics Express* 2012, 20, 22609-22615.
- [38] Kuyken B, Clemmen S, Kumar S, Bogaerts W, Van Thourhout D, Emplit P, Massar S, Roelkens G, Baets R On-chip parametric amplification with 26.5 dB gain at telecommunication wavelengths using CMOS-compatible hydrogenated amorphous silicon waveguides *Optics Letters* 2011, 36, 552-554.
- [39] Foster M, Turner AC, Sharping J, Schmidt B, Lipson M, Gaeta AL Broad-band optical parametric gain on a silicon photonic chip *Nature* 2006, 441, 960-963.
- [40] Ji H, Pu M, Hu H, Galili M, Oxenlřwe LK, Yvind K, Hvam JM, Jeppesen P Optical Waveform Sampling and Error-free Demultiplexing of 1.28 Tbit/s Serial Data in a Nano-engineered Silicon Waveguide *J. Lightwave Technol.* 2011, 29, 426-431.
- [41] Crandall RS Defect relaxation in amorphous silicon: Stretched exponentials, the Meyer-Neldel rule, and the Staebler-Wronski effect *Physical Review B* 1991, 43, 4057.
- [42] Fritzsche H, Development in understanding and controlling the Staebler-Wronski effect in a-Si: H Annual Review of Materials Research 2001, 31, 47-79.
- [43] Staebler DL, Wronski CR Reversible conductivity changes in discharge-produced amorphous Si *Applied Physics Letters* 1977, 31, 292-294.
- [44] Dave UD, Uvin S, Kuyken B, Selvaraja S, Leo F, Roelkens G Telecom to mid-infrared spanning supercontinuum generation in hydrogenated amorphous silicon waveguides using a Thulium doped fiber laser pump source *Optics Express* 2013, 21, 32032-32039.
- [45] Safioui J, Leo F, Kuyken B, Gorza SP, Selvaraja S, Baets R, Emplit P, Roelkens G, Massar S Supercontinuum generation in hydrogenated amorphous silicon waveguides at telecommunication wavelengths *Optics Express* 2014, 22, 3089-3097.
- [46] Wang KY, Velev VG, Fook K, Kowligly AS, Kumar P, Foster MA, Foster AC, Ping Y Multichannel photon-pair generation using hydrogenated amorphous silicon waveguides *Optics Letters* 2014, 39, 914-917.
- [47] S. Clemmen, A. Perret, S. K. Selvaraja, W. Bogaerts, D. van Thourhout, R. Baets, Ph. Emplit, and S. Massar, Generation of correlated photons in hydrogenated amorphous-silicon waveguide, *Optics Letters* 2010, 35, 3483-3485.
- [48] Wathen J, Vincent RP, Suess R, Wang KY, Foster AC, Murphy TE Non-instantaneous optical nonlinearity of an a-Si: H nanowire waveguide *Optics Express* 2014, 22, 22730-22742.
- [49] Yokoyama H, Tsubokawa H, Guo H, Shikata J, Sato K, Takashima K, Kashiwagi K, Saito N, Taniguchi H, Ito H Twophoton bioimaging utilizing supercontinuum light generated by a high-peak-power picosecond semiconductor laser source *J. Biomed.* 2007, 12, 054015-054019.
- [50] Ishida S, Nishizawa N, Ohta T, Itoh K Ultrahigh-Resolution Optical Coherence Tomography in 1.7  $\mu\text{m}$  Region with Fiber Laser Supercontinuum in Low-Water-Absorption Samples *Appl. Phys. Exp.* 2011, 4, 052501.
- [51] Mikami H, Shiozawa M, Shirai M, Watanabe K Compact light source for ultrabroadband coherent anti-Stoke Raman scattering (CARS) microscopy *Opt. Exp.* 2015, 23, 2872-2878.
- [52] Haolan Z, Kuyken B, Clemmen S, Leo F, Subramanian A, Dhakal A, Helin P Visible-to-near-infrared octave spanning supercontinuum generation in a silicon nitride waveguide *Optics Letters* 2015, 40, 2177-2180.
- [53] Lorenzo P, Lockwood DJ *Silicon photonics 2004*, Springer Science & Business Media.
- [54] De Vos K, Bartolozzi I, Schacht E, Bienstman P, Baets R Silicon-on-Insulator microring resonator for sensitive and label-free biosensing *Optics Express* 2007, 15, 7610-7615.

- [55] Robinson J, Chen L, Lipson M On-chip gas detection in silicon optical microcavities." *Optics Express* 2008, 16, 4296-4301.
- [56] Raghunathan V, Borlaug D, Rice RR, Jalali B Demonstration of a mid-infrared silicon Raman amplifier *Optics Express* 2007, 15, 14355-14362.
- [57] Kuyken B, Liu X, Osgood RM Jr, Baets R, Roelkens G, Green WMJ Mid-infrared to telecom-band supercontinuum generation in highly nonlinear silicon-on-insulator wire waveguides *Optics Express* 2011, 19, 20172-20181.
- [58] Kuyken B, Liu X, Roelkens G, Baets R, Osgood RM Jr, Green WMJ 50 dB parametric on-chip gain in silicon photonic wires *Optics letters* 2011, 36, 4401-4403.
- [59] Kovačević M, Acampora A Benefits of wavelength translation in all-optical clear-channel networks *IEEE Journal of Selected Areas in Communications* 1996, 14, 868-880.
- [60] Midwinter JE, Warner J Up-Conversion of Near Infrared to Visible Radiation in Lithium-meta-Niobate *Journal of Applied Physics* 1967, 38, 519-523.
- [61] Buchter KDF, Herrmann H, Langrock C, Fejer M, Sohler W All-optical Ti:PPLN wavelength conversion modules for free-space optical transmission links in the mid-infrared. *Optics Letters* 2009, 34, 470–472.
- [62] Dam JS, Pedersen C, Tidemand-Lichtenberg P High-resolution two-dimensional image upconversion of incoherent light *Optics Letters* 2010, 35, 3796–3798.
- [63] Liu, Xiaoping, Bart Kuyken, Gunther Roelkens, Roel Baets, Richard M. Osgood Jr, and William MJ Green. "Bridging the mid-infrared-to-telecom gap with silicon nanophotonic spectral translation." *Nature Photonics* 6, no. 10 (2012): 667-671.
- [64] Gholami F, Kuo B, Zlatanovic S, Alic N, Radic S Phase-preserving parametric wavelength conversion to SWIR band in highly nonlinear dispersion stabilized fiber *Optics Express* 2013, 21, 11415-11424.
- [65] Kuyken B, Verheyen P, Tannouri P, Liu X, Van Campenhout J, Baets R, Green WMJ, Roelkens G Generation of 3.6  $\mu\text{m}$  radiation and telecom-band amplification by four-wave mixing in a silicon waveguide with normal group velocity dispersion *Optics Letters* 2014, 39, 1349-1352.
- [66] Kuyken B, Ideguchi T, Holzner S, Yan M, Hansch TW, Van Campenhout J, Verheyen P, Coen S, Leo F, Baets R, Roelkens G, N. Picque An octave spanning mid-infrared frequency comb generated in a silicon nanophotonic wire waveguide *Nat. Commun.* 2015, 6, 6310.
- [67] Wang KY, Foster MA, Foster AC Wavelength-agile near-IR optical parametric oscillator using a deposited silicon waveguide *Optics Express* 2015, 23, 15431-15439.
- [68] Kuyken, Bart, Xiaoping Liu, Richard M. Osgood, Roel Baets, Günther Roelkens, and William MJ Green. "A silicon-based widely tunable short-wave infrared optical parametric oscillator." *Optics express* 21, no. 5 (2013): 5931-5940.
- [69] Jacobsen R, Andersen KN, Borel P, Fage-Pedersen J, Frandsen L, Hansen O, Kristensen M Strained silicon as a new electro-optic material *Nature* 2006, 441, 199-202.
- [70] Cazzanelli M, Bianco F, Borga E, Pucker G, Ghulinyan M, Degoli E, Luppi E Second-harmonic generation in silicon waveguides strained by silicon nitride *Nature materials* 2012, 11, 148-154.
- [71] Shin H, Qiu W, Jarecki R, Cox JA, Olsson RH, Starbuck A, Wang Z, Rakich PT Tailorable stimulated Brillouin scattering in nanoscale silicon waveguides *Nature communications* 2013, 4.
- [72] Van Laer R, Kuyken B, Van Thourhout D, Baets R Interaction between light and highly confined hypersound in a silicon photonic nanowire *Nature Photonics* 2015, 9, 199-203.
- [73] Van Laer et al. Net gain in a silicon photonic waveguide, to be published
- [74] Casas-Bedoya A, Morrison B, Pagani M, Marpaung D, Eggleton BJ Tunable narrowband microwave photonic filter created by stimulated Brillouin scattering from a Silicon nanowire *arXiv preprint arXiv:1506.07637* (2015).